PAPER

Check for updates

The impact of phenyl–phenyl linkage on the thermodynamic, optical and morphological behavior of carbazol derivatives†

José C. S. Costa, [iD] *[ab] Marco A. L. Lima, [iD] [a] Adélio Mendes [iD] [b] and Luís M. N. B. F. Santos [iD] *[a]

The impact of structural differentiation between phenylcarbazoles (**PhC**, **mCP**, **CBP**, **TCB**) and phenylamines (**TPA**, **BDB**, **TPB**, **TDAB**) on the phase equilibria, optical spectrum, band gap, and thin-film morphology is evaluated and discussed. The carbazolyl units lead to a lower electronic conjugation contributing to a wide band gap when compared with the diphenylamine analogs. The fusion and sublimation equilibria indicate that entropic contribution is the key factor for the distinguished melting behavior and solid-phase volatility between phenylcarbazole derivatives and phenylamine analogs. The molecular differentiation between the two classes of compounds is not reflected in the crystal packing and intermolecular interactions. However, compared with the diphenylamino groups, the incorporation of carbazolyl moieties contributes to a less flexible molecule. Moreover, the results evidence that intermolecular bonding disruption along the fusion transition is more extensive for phenylamine derivatives. Due to the asymmetric nonplanar structure, **mCP** is characterized by a ratio of $\{T_g/T_m \approx 3/4\}$ while the more symmetric **CBP** and **TCB** molecules display ratios closer to $\{T_g/T_m \approx 2/3\}$. Vapor-deposited thin films of **mCP**, **CBP**, and **TCB** are amorphous and their morphology is highly dependent on the substrate roughness. The lower flexibility of nonplanar phenylcarbazoles induces the formation of a glassy state due to the harder packing mechanism leading to the lower ability of the crystallization process.

Introduction

The allure of cheaper and more sustainable organic electronic devices such as solar cells (OPVs), field-effect transistors (OFETs) and light-emitting diodes (OLEDs) has brought the attention of the scientific community to investigate and develop stable organic semiconducting materials (OSCs).[1–5] Among the semiconductors, hole-transporting materials (HTMs) based on conductive small organic molecules have become one of the hottest topics in molecular electronics.[6–10] High-performance HTMs should exhibit high hole mobilities, a low potential of ionization and good thermal stability in the amorphous phase.[11–13] Amorphous materials consisting of phenylamine and/or carbazol moieties are usually incorporated as hole-transporting thin films in OLEDs and OPVs.[14–18] Thin films of diamine and triphenylamine derivatives (*e.g.*

TPD and NPB) are commonly used as the typical hole-transporting layers in OLEDs and efforts have been made to understand their thermophysical characteristics, with emphasis on thermal and transport properties in the thin film state.[19–22] Likewise, carbazole derivatives have also gathered research interest due to the low-cost and good charge transport ability of the carbazolyl moiety.[23–25] Carbazol unit provides a wide range of charge transport molecules, such as carbazole-based HTMs with triphenylamine moieties, which have been explored as promising candidates for high-performing perovskite solar cells.[26–28] Moreover, carbazole compounds are very relevant in developing phosphorescent organic light-emitting diodes (PHOLEDs), where these compounds act as the host materials, mainly due to their high triplet state energy and excellent hole transport capability.[29–31] Among the carbazole-based compounds, the 4,4′-bis(*N*-carbazolyl)-1,1′-biphenyl (**CBP**) and 1,3-bis(*N*-carbazolyl)benzene (**mCP**) have seen wide use in PHOLEDs, with interesting results in light-emitting cells.[32,33] In addition to molecular electronic devices, carbazol derivatives are exciting liquid organic hydrogen carriers (LOHCs) and have been investigating by different research groups aiming for sustainable industrial applications.[34–39] Despite carbazole derivatives having a recognized technological relevance for energy storage, there is a general lack of reports regarding their
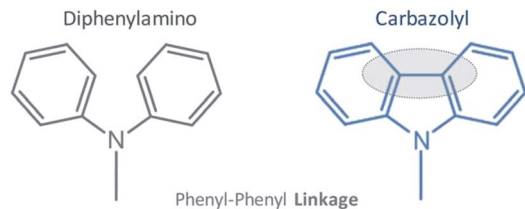
Fig. 1 Structural differentiation between diphenylamino and carba-zolyl moieties.

thermal behavior, including phase change properties and volatility studies. These properties are also of great importance for the manufacturing technology of thin films by vapor deposition procedures.[19,21,40–44] In previous works, thermo-physical, optical and morphological studies were carried out for an extended series of aromatic *N*-phenylamines.[19,21] *N*-Phenylcarbazoles have molecular structures analogous to the phenylamines, with an additional chemical bond between the phenyl groups (phenyl–phenyl linkage) in the carbazolyl unit (Fig. 1).[45,46]

In this context, the aim of this work is to acquire a better understanding of the impact of this molecular differentia-tion on the phase transition equilibria, optical spectrum, band gap, and morphological properties. The molecular structures of carbazol derivatives studied in this work (**PhC**, **mCP**, **CBP**, and **TCB**) are presented in Fig. 2. Molecular structures of corresponding phenylamines are depicted for comparison.
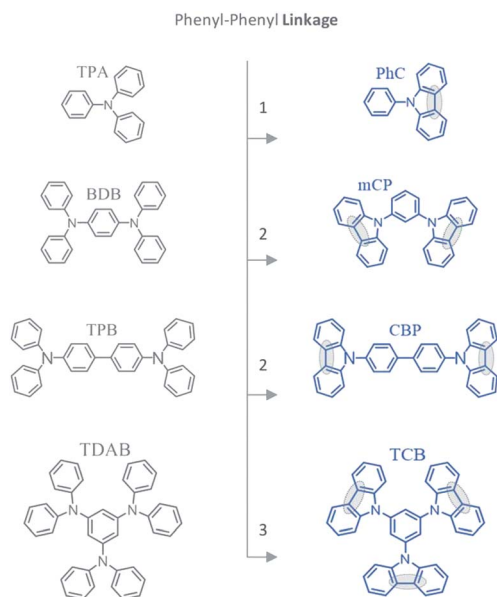

Fig. 2 Molecular structure of the materials studied and the adopted abbreviations: triphenylamine (TPA); 9-phenylcarbazole (PhC); 1,4-bis(diphenylamino)benzene (BDB); 1,3-bis(*N*-carbazolyl)benzene (mCP); tetra-*N*-phenylbenzidine (TPB); 4,4′-bis(*N*-carbazolyl)-1,1′-biphenyl (CBP); 1,3,5-tris(diphenylamino)benzene (TDAB); 1,3,5-tris(*N*-carbazolyl)benzene (TCB).

Experimental section

Materials

The materials studied, 1,3-bis(*N*-carbazolyl)benzene (**mCP**; CAS number 550378-78-4; mass fraction 0.997), 4,4′-bis(*N*-carba-zolyl)-1,1′-biphenyl (**CBP**; CAS number 58328-31-7; mass frac-tion 0.989), and 1,3,5-tris(*N*-carbazolyl)benzene (**TCB**; CAS number 148044-07-9; mass fraction 0.987) were commercially purchased from Sigma-Aldrich/Merck. To obtain high purity samples, the solids **CBP** and **TCB** were purified by sublimation under reduced pressure at $T = 548$ K and $T = 573$ K, respec-tively. Prior to fundamental studies and thin film deposition, the volatile content of **mCP**, **CBP**, and **TCB** were removed by vacuum thermal evaporation ($p < 10^{-4}$ Pa) at $T = 448$ K, $T = 473$ K, and $T = 523$ K, respectively. The high degree of purity (final mass fraction purity of 0.999) of the compounds was checked by gas–liquid chromatography, using an Agilent chromatograph model 4890D, equipped with an HP-5 column and a flame ionization detector (FID). The relative atomic masses used were those recommended by IUPAC.[47]

UV-visible absorption spectroscopy

UV-vis absorption properties of **mCP**, **CBP** and **TCB** were explored using a diode array spectrophotometer (Agilent 8543 UV-visible spectroscopy system). Absorption spectra in diluted solutions ($\approx 10^{-5}$ mol dm^{-3}) using CH$_2$Cl$_2$ as a solvent were recorded over the range of 200–700 nm, using quartz cells with a path length of 10.00 mm maintained at a constant tempera-ture of $T = 298.15$ K. Temperature control was attained by means of a refrigerated circulator. The optical band gap of each phenylcarbazole derivative was inferred from the offset wave-length of each UV-vis spectrum, according to the methodology described in a previous work.[4]

Differential scanning calorimetry (DSC)

The melting properties (melting temperatures and enthalpies associated to the solid-to-liquid phase transition) of **mCP**, **CBP** and **TCB** were explored in a heat flux differential scanning calorimeter (NETZSCH, DSC 200 F3 Maia) applying a constant flow of nitrogen (50 cm^3 min^{-1}), a heating rate of 2 K min^{-1} and using hermetically sealed aluminium crucibles (25 µl). For each material (samples of about 5 mg), at least four independent experiments were performed from $T = 298$ K to a temperature of 20 K higher than their melting temperature. The temperature and heat flux scales of the DSC were calibrated by an accurate determination of the temperature and the enthalpy of fusion of several reference materials[48,49] for thermal analysis (*o*-terphenyl, benzoic acid, indium, triphenylene, tin, perylene, zinc), and the compounds under study were measured using the same experimental method as in the calibration runs.

Knudsen effusion/volatility measurements

The volatility of **mCP**, **CBP**, and **TCB** was explored by a Knudsen effusion methodology based on a quartz crystal microbalance.[50] Requiring small amounts of sample and providing accurate

experimental data in low effusion times, this method has been commonly applied for the measurement of equilibrium vapor pressures of low volatile organic materials (0.01–1 Pa). The performance and accuracy of the Knudsen effusion approach was evaluated by measuring the equilibrium vapor pressures of 1,3,5-triphenylbenzene, an established reference organic compound for the enthalpy of sublimation and a recommended compound for sublimation studies at relatively high temperatures.[42,48–55] The vapor pressure of **mCP**, **CBP**, and **TCB** was determined at different temperature intervals: **mCP** (453.2 to 478.8 K); **CBP** (523.2 to 550.6 K); **TCB** (555.7 to 582.6 K).

Physical vapor deposition (PVD)

Thin films of **mCP**, **CBP**, and **TCB** were prepared through a customized procedure of PVD using the ThinFilmVD apparatus developed in our laboratory.[42] The procedural methodology and the capabilities of this technique have been presented in recent reports.[21,42,43,56,57] The materials studied were deposited on the surface of three different substrates (maintained at a constant temperature of 293 K): 6 MHz gold-coated quartz crystals; 6 MHz silver-coated quartz crystals; 6 MHz aluminium-coated quartz crystals. Based on the results of Knudsen effusion, thin films were deposited by thermal evaporation in high vacuum conditions ($<10^{-4}$ Pa) under the same experimental conditions: equilibrium vapor pressure of ≈ 0.3 Pa; mass flow rate at the substrate surface of ≈ 22 ng cm^{-2} s^{-1}; deposition time of 60 minutes; for these experimental conditions, **mCP**, **CBP** and **TCB** were evaporated at 472, 545, and 573 K, respectively. The substrates were cleaned with ethanol and dried with a pure and dry argon gas flow. Vapor-deposited thin film samples were stored in vacuum conditions to avoid contamination.

High-resolution scanning electron microscopy (SEM)

The topography of the vapor-deposited thin films was investigated by scanning electron microscopy (SEM) through the high-resolution FEI Quanta 400 FEG ESEM/EDAX Genesis X4M instrument at the CEMUP (Centro de Materiais da Universidade do Porto) services. SEM micrographs (top views) were acquired using a secondary electron detector (SE). The acceleration voltage was 10 keV, while an in-lens detector was employed with a working distance of about 10 mm.

Results and discussion

Optical properties

The optical properties of each carbazole derivative (diluted solution in CH$_2$Cl$_2$) were examined by means of UV-visible absorption spectroscopy. Fig. 3 presents the experimental UV-vis spectra of **mCP**, **CBP** and **TCB** (Fig. 3A) and the data for corresponding phenylamines (**TDAB** and **TPB**) are depicted for comparison (Fig. 3B and C). The detailed spectrum of each compound is presented as ESI.† Table 1 lists the experimental data for the absorption wavelengths at the maxima and corresponding molar absorptivities, absorption edge wavelengths and derived optical band gaps for a series of N-phenylcarbazoles
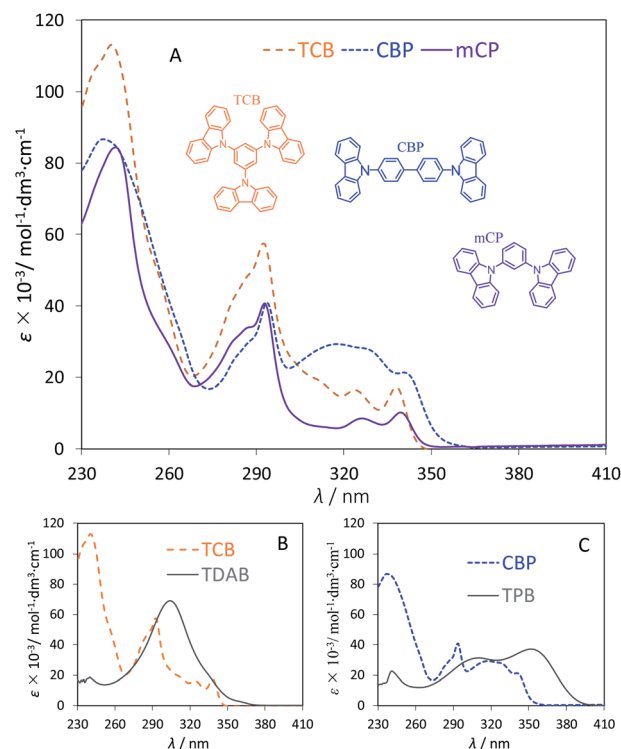

Fig. 3 UV-vis spectra, molar absorptivity (ε) as a function of wavelength (λ), recorded in CH$_2$Cl$_2$, at $T = 298.1$ K, for **mCP**, **CBP** and **TCB** (A) and UV-vis spectra comparing the carbazol derivative with its corresponding phenylamine: **TCB** *vs.* **TDAB** (B) and **CBP** *vs.* **TPB** (C).

Table 1 Wavelengths ($\lambda_{abs.max.}$) and molar absorptivities ($\varepsilon_{max.}$) at the maxima, absorption edge wavelengths ($\lambda_{abs.edge}$) and derived optical band gaps ($E_{optical\ gap}$) for the studied N-phenylcarbazoles (**mCP**, **CBP** and **TCB**). Values for the corresponding N-phenylamines are presented for comparison[4]

Material	$\lambda_{abs.max.}$, nm	$\varepsilon_{max.} \cdot 10^{-3}$, mol^{-1} dm^3 cm^{-1}	$\lambda_{abs.edge}$, nm	$E_{optical\ gap}$, eV
mCP	242	84	347	3.57
	293	41		
	326	9		
	339	10		
CBP	237	87	353	3.51
	294	41		
	318	29		
	341	21		
TCB	240	113	345	3.59
	292	57		
	324	16		
	338	17		
BDB[a]	241	16	390	3.19
	315	30		
TPB[a]	241	23	400	3.11
	310	31		
	351	37		
TDAB[a]	240	19	375	3.31
	304	69		

[a] Data from ref. 4.

(**mCP, CBP** and **TCB**) and corresponding *N*-phenylamines (**BDB, TPB,** and **TDAB**). The UV-vis spectra exhibit absorption peaks in the ultraviolet region (<350 nm) as a result of electronic transitions occurring due to the interaction of radiation with the molecules studied. The so-called "optical gap" of each material can be derived from each spectrum through the onset of the long-wavelength absorption maxima.[4,58] Four main absorption peaks, centred at ≈ 240, 293, 325 and 340 nm, respectively, are observed (Fig. 3A) for each carbazole derivative studied (**mCP, CBP** and **TCB**), without any significant bathochromic shift being perceived. Absorption peaks located at the same wavelengths were observed for a diluted solution of 9-phenylcarbazole (**PhC**) in DCM.[59] The absorption peak located at ≈ 293 nm is appointed to $\pi \to \pi^*$ electronic transition, whereas the peaks located at ≈ 326 nm and ≈ 340 nm are assigned to n $\to \pi^*$ electronic transitions.[59] The absorption peaks relative to $\pi \to \pi^*$ transition of **mCP** and **CBP** display similar values of molar absorptivity as both molecules present the same number of carbazolyl units.

The presence of more chromophore groups in **TCB**, which is constituted by three carbazolyl units, leads to the overlap of the absorption peaks and, consequently, a hyperchromic effect is clearly noted.

The experimental results also indicate that the presence of two central aromatic rings in **CBP** leads to a hyperchromic effect of the absorption bands peaking at 318 and 341 nm as well as to a reduced optical band gap energy. A comparative analysis between the UV-vis spectra of phenylcarbazoles and phenylamines (Fig. 3B and C) evidences a higher degree of electronic conjugation in **TDAB** and **TPB** in comparison with **TCB** and **CBP**. Hence, the additional chemical bond between the phenyl groups of the carbazolyl units leads to clear hypsochromic shifts on the absorption UV-vis absorption bands and, consequently, to a higher band gap energy. According to recent reports, the short conjugation of carbazole derivatives leading to a wide band gap is a key factor for the high triplet energy presented by this class of semiconductors.[24,60–63] Optical band gaps (E_g) of 3.57, 3.51 and 3.59 eV were estimated from the absorption edge wavelengths ($\lambda_{abs.edge}$) of the UV-vis spectra for **mCP, CBP** and **TCB**, respectively ($E_g \approx 1240/\lambda_{abs.edge}$). These values are in nice agreement with literature reports presented by other authors for samples studied in DCM solution and/or in the thin-film state. There are no significant deviations between the values determined in the solution or in the thin film. In fact, carbazole derivatives are materials of relative low polarity and do not establish very specific intermolecular interactions. Moreover, DCM is a suitable solvent that dissolves these materials without affecting their optical behavior, whereby the molecular environment in diluted solutions of carbazole derivatives and in amorphous thin film state can be comparable.

Thermodynamic properties of fusion

An accurate analysis of the melting properties was carried out to evaluate the relative stability of the solid phase in terms of its fusion process. The thermodynamic properties associated with the solid–liquid phase equilibrium of all compounds depicted

Table 2 Thermodynamic properties associated to the solid–liquid equilibrium of PhC, mCP, CBP, TCB, TPA, BDB, TPB, and TDAB: melting temperatures (T_m), standard molar enthalpies ($\Delta_{fus}H^\circ$) and entropies ($\Delta_{fus}S^\circ$) of fusion at the melting temperature and derived thermodynamic properties of fusion ($\Delta_{fus}H^\circ$, $\Delta_{fus}S^\circ$, and $\Delta_{fus}G^\circ$) at $\theta =$ 298.15 K. Experimental results and literature data

Material	T_m, K	$\Delta_{fus}H^\circ(T_m)$, kJ mol^{-1}	$\Delta_{fus}S^\circ(T_m)$, J K^{-1} mol^{-1}
PhC[a]	367.9 ± 0.3	19.4 ± 0.3	52.7 ± 0.8
mCP	453.8 ± 0.2	27.1 ± 1.4	59.8 ± 2.5
CBP	553.5 ± 1.2	42.7 ± 2.8	77.2 ± 4.1
TCB	597.5 ± 1.2	41.7 ± 2.5	69.9 ± 4.2
TPA[b]	400.2 ± 0.5	24.9 ± 0.5	62.2 ± 1.2
BDB[c]	475.4 ± 0.2	44.1 ± 0.4	92.7 ± 0.8
TPB[c]	504.6 ± 0.1	46.2 ± 0.3	91.5 ± 0.6
TDAB[c]	526.3 ± 0.1	62.1 ± 0.8	117.9 ± 1.5

	Values at $\theta =$ 298.15 K		
	$\Delta_{fus}G^\circ$	$\Delta_{fus}H^\circ$	$\Delta_{fus}S^\circ$
PhC	3.3 ± 1.0	15.9 ± 0.8	42.2 ± 2.3
mCP	7.8 ± 2.6	19.4 ± 2.1	38.8 ± 4.9
CBP	16.2 ± 4.4	30.0 ± 3.8	46.3 ± 7.4
TCB	16.3 ± 4.6	26.8 ± 3.9	35.1 ± 8.1
TPA	5.6 ± 1.5	19.8 ± 1.1	47.5 ± 3.2
BDB	14.6 ± 2.3	35.2 ± 1.8	69.4 ± 4.7
TPB	16.4 ± 2.6	35.9 ± 2.1	65.2 ± 5.3
TDAB	24.0 ± 3.0	50.7 ± 2.4	89.5 ± 5.9

[a] Data from ref. 39. [b] Data from ref. 67. [c] Data from ref. 19.

in Fig. 2 are listed in Table 2. Melting temperatures (T_m) and standard molar enthalpies of fusion ($\Delta_{fus}H^\circ$) were directly obtained from DSC experimental data (determined by the integration of the area under the endothermic curve considering the initial and end inflections of the central peak), and the standard molar entropies of fusion ($\Delta_{fus}S^\circ$) were derived as $\Delta_{fus}S^\circ = \Delta_{fus}H^\circ/T_m$. Heat capacity corrections were developed to determine hypothetical thermodynamic properties at 298.15 K. This adjustment was made to evaluate and compare the thermochemical properties of a series of compounds in a more accurate fashion, by establishing the same reference temperature.[64,65] The heat capacity corrections of the enthalpies ($\Delta_{fus}H^\circ$), entropies ($\Delta_{fus}S^\circ$) and Gibbs energies ($\Delta_{fus}G^\circ$) of fusion to the reference temperature of $\theta =$ 298.15 K, for each phenylcarbazole or phenylamine, were calculated using the eqn (1), (2), and (3), respectively. Following previous reports, the typical and recommended value of $\Delta_{fus}C_p^\circ = (50 \pm 10)$ J K^{-1} mol^{-1} was used as the difference between the liquid and solid phase heat capacity at 298.15 K.[19,21,66] In Table 2, the values of T_m and $\Delta_{fus}H^\circ$ for **PhC, TPA, BDB, TPB,** and **TDAB** were obtained from literature and are listed for comparison.[19,21,39,67] Fig. 4 presents an evaluation of the magnitude of enthalpies and entropies of fusion for phenylcarbazoles and phenylamines. The comparison between **TPA** and **PhC, TPB** and **CBP,** and **TDAB** and **TCB** evidences that both values of $\Delta_{fus}H^\circ$ and $\Delta_{fus}S^\circ$ (at the same reference temperature) are clearly higher for phenylamines. The
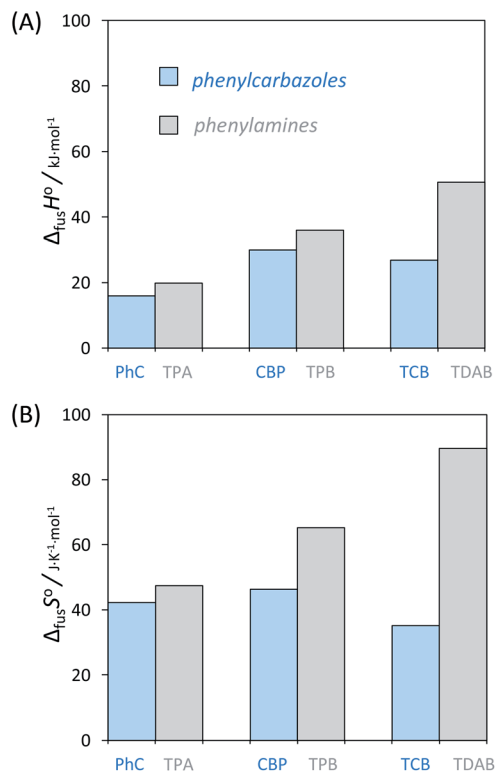
Fig. 4 Schematic representation for the magnitude of enthalpies ($\Delta_{\text{fus}}H°$, (A)) and entropies ($\Delta_{\text{fus}}S°$, (B)) of fusion, at $\theta = 298.15$ K, for series of phenylcarbazoles (**PhC**, **CBP**, **TCB**) and phenylamines (**TPA**, **TPB**, **TDAB**).

relative stability of a solid phase, in terms of its solid-to-liquid phase transition, is typically evaluated by the magnitude of melting temperature, which results in a balance between enthalpic and entropic contributions.[64] The melting temperature of a material can be derived as $T_{\text{m}} = \Delta_{\text{fus}}H°(T_{\text{m}})/\Delta_{\text{fus}}S°(T_{\text{m}})$. Hence, higher values of $\Delta_{\text{fus}}H°$ and lower values of $\Delta_{\text{fus}}S°$ lead to higher melting temperatures. From a comparative analysis between melting points of phenylcarbazoles and their phenylamine analogues, the following conclusions can be drawn: T_{m} of **PhC** is 32 K lower than **TPA**; T_{m} of **CBP** is 49 K higher than **TPB**; T_{m} of **TCB** is 71 K higher than **TDAB**. These findings, together with the data represented in Fig. 4, indicate that entropic contribution is the preponderant thermodynamic property for the differentiation between melting temperatures of phenylcarbazoles and phenylamines. In addition, and contrary to observed between **TPB** and **TDAB** where **TDAB** displays higher values of $\Delta_{\text{fus}}H°$ and $\Delta_{\text{fus}}S°$, a comparison between **CBP** and **TCB** shows lower values of $\Delta_{\text{fus}}H°$ and $\Delta_{\text{fus}}S°$ for **TCB**. Due to enthalpy–entropy compensation, in both cases, the compounds with higher molar mass are characterized by larger values of T_{m}.

$$\Delta_{\text{fus}}H°(\theta) = \Delta_{\text{fus}}H°(T_{\text{m}}) + \Delta_{\text{fus}}C_{\text{p}}° \times (\theta - T_{\text{m}}) \tag{1}$$

$$\Delta_{\text{fus}}S°(\theta) = \frac{\Delta_{\text{fus}}H°(T_{\text{m}})}{T_{\text{m}}} + \Delta_{\text{fus}}C_{\text{p}}° \times \ln\left(\frac{\theta}{T_{\text{m}}}\right) \tag{2}$$

$$\Delta_{\text{fus}}G°(\theta) = \Delta_{\text{fus}}H°(T_{\text{m}})\left[1 - \frac{\theta}{T_{\text{m}}}\right]$$

$$+\Delta C_{\text{p}}°\left[\theta\left(1 - \ln\left(\frac{\theta}{T_{\text{m}}}\right)\right) - (T_{\text{m}})\right] \tag{3}$$

The phenylcarbazoles **mCP** and **TCB** result from the introduction of additional carbazole groups in *meta* position into the **PhC** moiety. That way, we can conclude that the increment of carbazolyl units (in phenylcarbazoles) is followed by increased values of T_{m} and $\Delta_{\text{fus}}H°$. In this case, both enthalpic and entropic factors are contributing to increasing T_{m}, as the magnitude of $\Delta_{\text{fus}}S°$ is lower when more carbazoles are included.

Thermodynamic properties of sublimation/vaporization

The solid–gas equilibria of **CBP** and **TCB** and the liquid–gas equilibrium of **mCP** were evaluated determining the equilibrium vapor pressures of the compounds in temperature intervals of about 25 K using the Knudsen effusion procedure (Table 3). The accuracy of the methodology was tested with 1,3,5-triphenylbenzene; the relative deviations between experimental and

Table 3 Experimental vapor pressures of **mCP** (liquid), **CBP** (solid) and **TCB** (solid) obtained with the quartz crystal microbalance Knudsen effusion methodology

T/K	p/Pa	Δp/Pa	T/K	p/Pa	Δp/Pa
mCP (liquid)					
453.20	0.0770	−0.0003	469.70	0.2740	0.0014
456.20	0.0975	−0.0003	471.20	0.3040	−0.0003
459.20	0.1240	0.0005	472.70	0.3420	0.0024
462.20	0.1560	0.0006	474.20	0.3740	−0.0046
465.20	0.1950	0.0001	475.70	0.4260	0.0042
466.70	0.2180	−0.0002	477.20	0.4630	−0.0067
468.20	0.2440	0.0001	478.80	0.5290	0.0027
CBP (solid)					
523.20	0.0519	0.0006	540.50	0.2093	0.0003
525.55	0.0615	−0.0009	542.40	0.2420	−0.0005
528.30	0.0788	0.0004	543.40	0.2630	0.0009
530.55	0.0935	−0.0007	545.50	0.3093	0.0009
533.33	0.1183	0.0002	546.50	0.3340	0.0009
535.55	0.1405	−0.0006	548.20	0.3740	−0.0055
536.40	0.1520	0.0009	549.50	0.4190	−0.0001
538.30	0.1760	0.0003	550.60	0.4580	0.0025
539.40	0.1920	0.0004			
TCB (solid)					
555.70	0.0785	−0.0004	569.50	0.2260	0.0010
558.35	0.0965	−0.0003	570.60	0.2440	0.0000
560.70	0.1150	−0.0010	572.35	0.2780	0.0004
561.50	0.1240	0.0007	573.35	0.2990	0.0003
563.35	0.1420	0.0001	575.60	0.3510	−0.0009
564.50	0.1550	0.0002	576.50	0.3760	0.0004
565.70	0.1690	−0.0004	578.35	0.4270	−0.0022
566.50	0.1820	0.0021	579.50	0.4670	0.0009
567.50	0.1940	0.0001	582.60	0.5780	−0.0032
568.35	0.2070	0.0004			

recommended vapor pressures were found to be less than 2%. In addition, the derived sublimation enthalpies ($\Delta_{sub}H° = 147.5 \pm 1.0$ kJ mol^{-1}) and entropies ($\Delta_{sub}S° = 251.3 \pm 2.3$ J K^{-1} mol^{-1}) for 1,3,5-triphenylbenzene, at $\theta = 298.15$ K, agree with the literature values.[42,48–55] Details are presented as ESI.† The dependence of vapor pressures with the effusion temperature was used to derive thermodynamic properties of phase transition; considering the mean temperature of each experiment, $\langle T \rangle$, molar enthalpies of sublimation (for **CBP** and **TCB**, $\Delta_{sub}H°$) and molar enthalpies of vaporization (for **mCP**, $\Delta_{vap}H°$) were derived using the integrated form of the Clausius–Clapeyron equation, where a is a constant and $b = \Delta_{sub;vap}H°(\langle T \rangle)/R$, eqn (4).

$$\ln(p/\text{Pa}) = a - b \times [(1/T)/\text{K}^{-1}] \quad (4)$$

The plots of $\ln(p) = f(1/T)$ for **mCP**, **CBP** and **TCB** are shown in Fig. 5. Table 4 lists the parameters of the Clausius–Clapeyron equation (a and b) with associated standard deviations, the effusion temperatures interval and equilibrium vapor pressures (EVP), and the standard molar enthalpies, $\Delta_{sub;vap}H°(\langle T \rangle)$, entropies, $\Delta_{sub;vap}S°(\langle T \rangle)$, and Gibbs energies, $\Delta_{sub;vap}G°(\langle T \rangle)$, of sublimation/vaporization at the mean temperature. $\Delta_{sub;vap}H°(\langle T \rangle)$ was determined from the parameter b of the eqn (4) and $\Delta_{sub;vap}S°(\langle T \rangle)$ were calculated using eqn (5). $\Delta_{sub;vap}G°(\langle T \rangle)$ was derived as $\{\Delta H°(\langle T \rangle) - \langle T \rangle \cdot \Delta S°(\langle T \rangle)\}$. Heat capacity corrections were made to determine molar enthalpies and entropies of sublimation (at $\theta = 298.15$ K), for solids **CBP** and **TCB**. The value of $\Delta_{sub}C_p° = (-20 \pm 10)$ J K^{-1} mol^{-1} was used as the difference between the gas and solid phase heat capacity at $\theta = 298.15$ K. The estimation of $\Delta_{sub}C_p°(\theta = 298.15$ K) was based on previous determinations of solid heat capacities of compounds with similar chemical structure, such as the phenylamines **TPB** and **TPD**, whose obtained values of $\Delta_{sub}C_p°$, are (-17.8 ± 10) and (-20.2 ± 10) J K^{-1} mol^{-1}, respectively.[19]

The value of $\Delta_{vap}C_p° = (70 \pm 10)$ J K^{-1} mol^{-1} obtained as $(\Delta_{sub}C_p° - \Delta_{fus}C_p°)$, was used as the difference between the gas
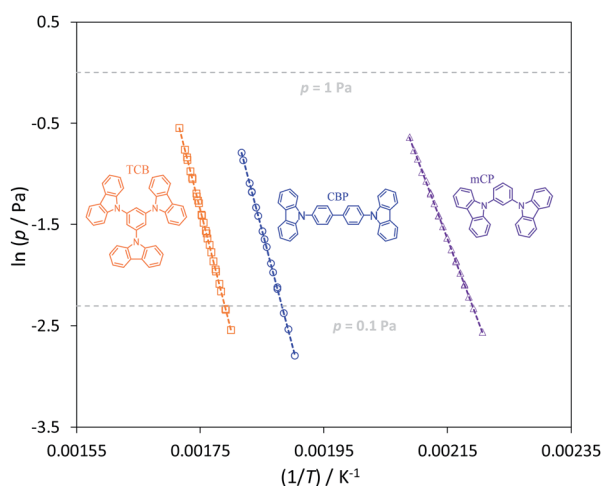
Table 4 Standard ($p° = 10^5$ Pa) thermodynamic properties (values at the mean temperature of the effusion experiments) associated to the liquid–gas equilibrium of **mCP** and to the solid–gas equilibria of **CBP** and **TCB**: effusion temperatures ($T_{effusion}$), equilibrium vapor pressures (EVP), and enthalpies ($\Delta_{sub;vap}H°$), entropies ($\Delta_{sub;vap}S°$) and Gibbs energies ($\Delta_{sub;vap}G°$) of phase transition. Parameters a and b were obtained from the integrated form of Clausius–Clapeyron equation

Property	**mCP** (l)	**CBP** (s)	**TCB** (s)
a	33.3 ± 0.1	40.9 ± 0.1	40.7 ± 0.1
b	$16\,263 \pm 54$	$22\,954 \pm 62$	$24\,029 \pm 48$
$T_{effusion}$	454 to 478	524 to 550	556 to 583
EVP	0.077 to 0.53	0.052 to 0.46	0.079 to 0.58
$\Delta_{sub;vap}H°$	135.2 ± 0.5	190.9 ± 0.5	199.9 ± 0.4
$\Delta_{sub;vap}S°$	181.3 ± 1.0	244.4 ± 1.0	242.8 ± 0.7
$\Delta_{sub;vap}G°$	81.1 ± 0.5	118.0 ± 0.6	127.5 ± 0.5

and liquid phase heat capacity at $\theta = 298.15$ K for the liquid **mCP**. The standard molar enthalpies and entropies of sublimation/vaporization, at the reference temperature of $\theta = 298.15$ K, were determined by eqn (6) and (7). $\Delta_{sub;vap}G°(\theta)$ was derived as $\{\Delta_{sub;vap}H°(\theta) - \theta \cdot \Delta_{sub;vap}S°(\theta)\}$. Thermodynamic parameters associated with the equilibria processes of fusion, sublimation, and vaporization, at the reference temperature θ, are interconnected by means of eqn (8). Sublimation and vaporization properties, at $\theta = 298.15$ K, are listed in Table 5.

$$\Delta_{sub}S°(\langle T \rangle, p(\langle T \rangle)) = \frac{\Delta_{sub}H°(\langle T \rangle)}{\langle T \rangle} - R \ln\left(\frac{p°}{p(\langle T \rangle)}\right) \quad (5)$$

Table 5 Standard molar enthalpies ($\Delta H°$), entropies ($\Delta S°$), and Gibbs energies ($\Delta G°$) of sublimation and vaporization, at $\theta = 298.15$ K, for **mCP**, **CBP**, and **TCB**. Literature values for **PhC**, **BDB**, **TPB**, and **TDAB** are listed for comparison

Material	$\Delta H°$, kJ mol^{-1}	$\Delta S°$, J K^{-1} mol^{-1}	$\Delta G°$, kJ mol^{-1}
Sublimation			
PhC[a]	116.1 ± 1.7	211.3 ± 5.0	53.1 ± 2.3
mCP	166.5 ± 2.7	251.7 ± 6.7	91.4 ± 3.4
CBP	195.7 ± 2.5	256.2 ± 6.0	119.3 ± 3.0
TCB	205.3 ± 2.7	255.8 ± 6.5	129.0 ± 3.4
TPA[b]	92.0 ± 2.5		
BDB[c]	178.8 ± 1.6	292.4 ± 4.3	91.7 ± 2.0
TPB[c]	198.5 ± 2.0	294.0 ± 5.2	110.9 ± 2.5
TDAB[c]	200.8 ± 2.0	298.1 ± 5.2	111.9 ± 2.5
Vaporization			
PhC	100.2 ± 1.9	169.1 ± 5.5	49.8 ± 2.5
mCP	147.1 ± 1.8	212.9 ± 4.6	83.6 ± 2.2
CBP	165.7 ± 4.5	209.9 ± 9.5	103.1 ± 5.4
TCB	178.5 ± 4.8	220.7 ± 10.4	112.7 ± 5.7
TPA	72.2 ± 3.2		
BDB	143.6 ± 2.4	223.0 ± 6.4	77.1 ± 3.0
TPB	162.6 ± 2.9	228.8 ± 7.4	94.5 ± 3.6
TDAB	150.1 ± 3.1	208.6 ± 7.8	87.9 ± 3.9

Fig. 5 Plots of $\ln(p)$ versus $1/T$ for **mCP** (triangles), **CBP** (circles) and **TCB** (squares).

[a] Data from ref. 39. [b] Data from ref. 68. [c] Data from ref. 19.

$$\Delta_{sub}H^{\circ}(\theta) = \Delta_{sub}H^{\circ}(\langle T \rangle) + \Delta_{sub}C^{\circ}_{p} \times (\theta - \langle T \rangle) \qquad (6)$$

$$\Delta_{sub}S^{\circ}(\theta) = \Delta_{sub}S^{\circ}(\langle T \rangle, p(\langle T \rangle)) + \Delta_{sub}C^{\circ}_{p} \times (\theta - \langle T \rangle) \qquad (7)$$

$$\Delta_{sub}[H^{\circ};S^{\circ};G^{\circ}] = \Delta_{vap}[H^{\circ};S^{\circ};G^{\circ}] + \Delta_{fus}[H^{\circ};S^{\circ};G^{\circ}] \qquad (8)$$

The experimental results of Table 3 and Fig. 5 evidence a volatility differentiation between **mCP**, **CBP** and **TCB**. The data for **mCP** corresponds to the liquid phase; the vapor pressures of solid **mCP** at the triple point are very low and outside the measuring range of the Knudsen apparatus (0.1 to 1 Pa).[50] The higher volatility of **CBP**, in comparison with **TCB**, was found to be enthalpically driven (entropies of sublimation are similar) indicating stronger cohesive energies in the crystalline phase of **TCB**. Comparing to their phenylamine analogues, the solid phase of phenylcarbazoles is less volatile presenting higher stability: **CBP** is less volatile than **TPB**; **TCB** is less volatile than **TDAB**. These results are highlighted by the higher values of $\Delta_{sub}G^{\circ}$ exhibited by phenylcarbazole derivatives. The values listed in Table 5 are useful to compare the relative stability of the condensed phases of all compounds. Concerning the solid phase, higher cohesive energies of **TPA**, in comparison with **PhC**, can be perceived from the magnitude of $\Delta_{sub}H^{\circ}$ values. For the other pairs of compounds (phenylcarbazole *vs.* phenylamine congener) there is no significant differentiation when comparing the $\Delta_{sub}H^{\circ}$, as deviations are less than 5 kJ mol⁻¹: 195.7 and 198.5 kJ mol⁻¹ for **CBP** and **TPB**, respectively; 205.3 and 200.8 kJ mol⁻¹ for **TCB** and **TDAB**, respectively. The experimental data indicate that the differentiation in the molecular structure of phenylcarbazoles and phenylamines does not affect significantly the crystal packing and intermolecular interactions. Hence, the noticeable difference that explains the lower volatility of solid phenylcarbazoles is the entropy of sublimation. Curiously, attending to the experimental uncertainties, the phenylcarbazole derivatives **mCP**, **CBP** and **TCB** have similar values of $\Delta_{sub}S^{\circ}$ (from 251.7 to 256.2 J K⁻¹ mol⁻¹). Comparatively, the solid phase of phenylamines **DDP**, **TPB** and **TDAB** have higher values of $\Delta_{sub}S^{\circ}$, but also similar between them (from 292.4 to 298.1 J K⁻¹ mol⁻¹). These results are consistent with fusion results indicating a clear entropic differentiation of phenylcarbazoles and phenylamines with respect to their liquid and gas phases. The additional chemical bond between the phenyl groups in the carbazolyl units leads to a less flexible chemical structure with a significant decrease of translational and rotational motions of the rings. The 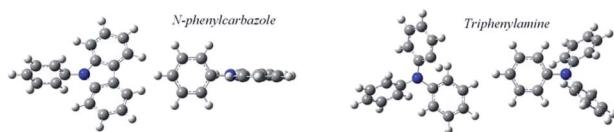most stable conformations of *N*-phenylcarbazole and triphenylamine are depicted in Fig. 6. In comparison to phenylamines, the more rigid phenylcarbazole derivatives exhibit lower absolute entropies in liquid and gas phases and thus, lower values of $\Delta_{fus}S^{\circ}$ and $\Delta_{sub}S^{\circ}$. Fig. 7 systematizes an additive scheme representing the increments in $\Delta_{sub}H^{\circ}$ and $\Delta_{sub}S^{\circ}$ (at the same reference temperature) upon successive introduction of carbazolyl or diphenylamino groups. The enthalpic increments between biphenyl and **CBP** and between biphenyl and **TPB** were found to be similar (114.2 and 117.0 kJ mol⁻¹), whereas a large differentiation is found by analysing the $\Delta_{sub}S^{\circ}$ increments (75.9 *vs.* 113.7 J K⁻¹ mol⁻¹). A comparison between **PhC**, **mCP**, and **TCB** shows that increments in $\Delta_{sub}H^{\circ}$ arising from the successive introductions of carbazolyl moieties decrease due to intramolecular repulsions between the groups. The same effect is observed when analysing the effect of introducing additional diphenylamino groups in **TPA**. The clear entropic differentiation between phenylcarbazoles and phenylamines is well emphasized by comparing the additive scheme for $\Delta_{sub}S^{\circ}$: lower values are systematically observed for derivatives containing carbazolyl moieties replacing diphenylamino groups. Concerning the phenylcarbazoles, to better elucidate the effect of incorporating carbazolyl groups in *meta* position on the sublimation thermodynamic properties of sublimation, Fig. 8 shows the dependence of $\Delta_{sub}H^{\circ}$, $T \cdot \Delta_{sub}S^{\circ}$, and $\Delta_{sub}G^{\circ}$ with the number of carbazolyl moieties. A linear dependence is observed for $\Delta_{sub}H^{\circ}$ values indicating a large intensity of intermolecular interactions in the lattice for **TCB**.

The relative stability of the solid phase of phenylcarbazole derivatives is mostly enthalpically driven and increases linearly with the molar mass (carbazolyl groups). The same conclusion was reached in a recent work for a series of phenylamine
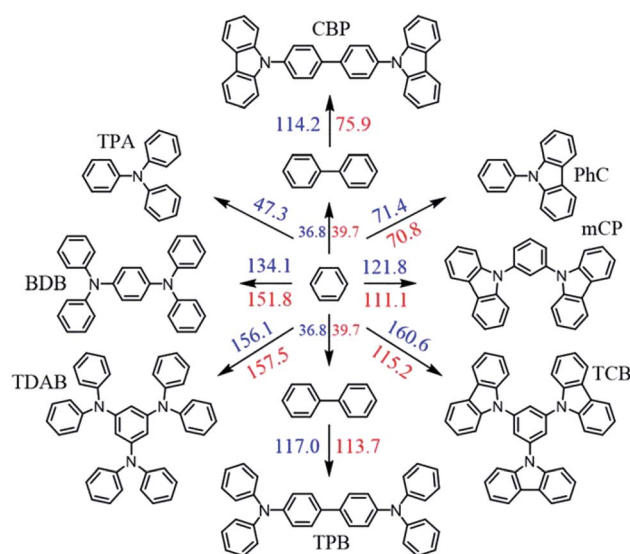

Fig. 6 Views of the B3LYP/6-31+G(d,p)-optimized structures of the minimum energy conformers of *N*-phenylcarbazole and triphenylamine.

Fig. 7 Additive scheme for $\Delta_{sub}H^{\circ}$ (298.15 K) (blue values, in kJ mol⁻¹) and $\Delta_{sub}S^{\circ}$ (298.15 K) (red values, in J K⁻¹ mol⁻¹), representing the increments in these quantities upon successive introduction of carbazolyl or diphenylamino groups. The errors in the calculated increments are omitted for clarity. $\Delta_{sub}H^{\circ}$ and $\Delta_{sub}S^{\circ}$ values for benzene (44.7 kJ mol⁻¹ and 140.6 J K⁻¹ mol⁻¹) and biphenyl (81.5 and 180.3 J K⁻¹ mol⁻¹) were obtained from literature.[69]
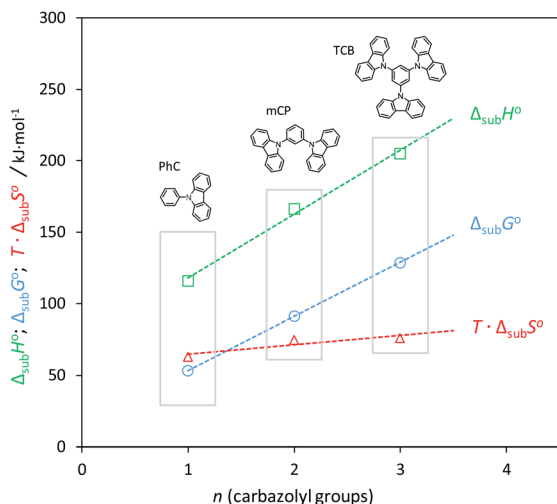
Fig. 8 Dependence of the thermodynamic properties of sublimation with the number of carbazolyl groups: $\Delta_{sub}H°$ (squares); $T\cdot\Delta_{sub}S°$ (triangles); $\Delta_{sub}G°$ (circles).

Fig. 9 $\Delta_{fus}H°/\Delta_{sub}H°$ ratios (blue solid circles and triangles) and $\Delta_{fus}S°/\Delta_{sub}S°$ ratios (red open circles and triangles) for series of phenyl-carbazoles (circles) and phenylamines (triangles). The thermodynamic properties were derived at $\theta = 298.15$ K.

derivatives with a different number of diphenylamino groups.[21] According to Fig. 8, there is no clear entropic differentiation along with the series and the enthalpy–entropy compensation leads to a highly linear dependence ($r^2 > 0.9999$) observed for $\Delta_{sub}G°$ values. The vaporization results, derived from the combination of fusion and sublimation data, were used to evaluate the relative stability of the liquid state. Looking at the sublimation and fusion data, there are clear entropic differentiations between phenylcarbazoles and their corresponding phenylamines. This distinction, however, is not so obvious for $\Delta_{vap}S°$ values. Moreover, there is a clear enthalpy–entropy compensation that explains the higher volatility of the liquid phase of phenylamines: when comparing each pair of congener compounds (**CBP** *vs.* **TPB** and **TCB** *vs.* **TDAB**), $\Delta_{vap}G°$ is higher for the compounds containing carbazolyl moieties; **CBP** and **TPB** display similar values of $\Delta_{vap}H°$; compared to **TDAB**, **TCB** is characterized by a higher value $\Delta_{vap}H°$ which arises from the larger differentiation in the fusion enthalpies of these compounds. In fact, compared to other molecules, **TDAB** requires a larger amount of energy to melt (≈ 62 kJ mol^{-1} at T_m). The enthalpic and entropic factors associated with differentiation in terms of intermolecular interactions and molecular flexibility can be explored in more detail by inferring the cohesive energies in the liquid phase. As discussed in recent works, a liquid with a significant level of structuration displays a low ratio of $\Delta_{fus}H°/\Delta_{sub}H°$ as most of the intermolecular interactions are not disrupted even after a melting process.[64,70] A similar effect is observed for phenylcarbazoles (Fig. 9).

In order to rationalize this effect emphasizing the structural differentiation of carbazoles and phenylamines, Fig. 9 represents the magnitude of {$\Delta_{fus}H°/\Delta_{sub}H°$} and {$\Delta_{fus}S°/\Delta_{sub}S°$} ratios for the studied compounds. Both ratios are clearly lower for phenylcarbazoles. The chemical bond between the phenyl groups in the carbazolyl unit contributes to a substance with a higher level of structuration and organization in the liquid
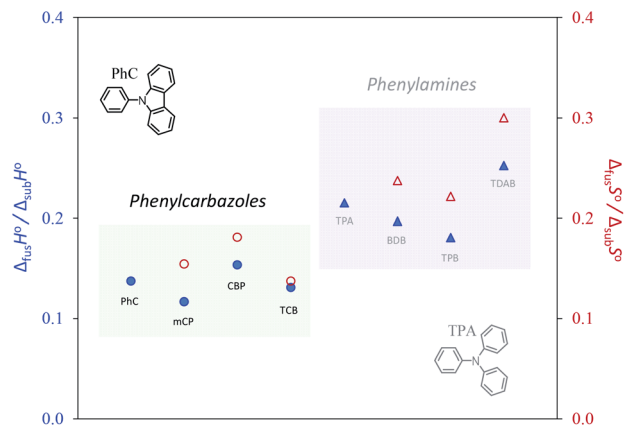
phase as in comparison with phenylamines, molecules are more rigid and available to perform more stable and powerful intermolecular interactions. For instance, $\Delta_{fus}H°/\Delta_{sub}H°$ ratios of 0.25 and 0.13 were found for **TDAB** and **TCB**, respectively; compared to **TCB**, the high flexibility of **TDAB** is also expressed by a larger ratio of $\Delta_{fus}S°/\Delta_{sub}S°$ (0.30 for **TDAB** *vs.* 0.14 for **TCB**). The results clarify that intermolecular bonding disruption along the fusion transition is more extensive for phenylamine derivatives.

Characterization of thin films

Based on volatility studies, thin films of **mCP**, **CBP**, and **TCB** were prepared by physical vapor deposition. A customized procedure of vacuum thermal evaporation has been used. SEM micrographs of vapor-deposited thin films onto quartz crystal surfaces coated with gold (Au), silver (Ag) or aluminium (Al) are presented by Fig. 10. The mass flow rate (φ, ng cm^{-2} s^{-1}) can be estimated according to eqn (9), in which $\varphi_{substrate}$ and $\varphi_{Knudsen\ cell}$ are the mass flow rates on the substrate surface and from the Knudsen cell orifice, respectively. This equation considers a geometrical factor g that is dependent on the distance between the deposition source (Knudsen cell) and the deposition surface (substrate). For the calculation of $\varphi_{Knudsen\ cell}$, T is the evaporation temperature, p is the equilibrium vapor pressure at T, w_o is a transmission probability factor, M_M is the molar mass of the vapor effused, R is the gas constant, m is the mass of sample evaporated, t is the deposition time, and A_o is the area of the Knudsen cell orifice.

$$\varphi_{substrate} = g\varphi_{Knudsen\ cell} = g\frac{pw_o\left(M_M^{1/2}\right)}{(2\pi RT)^{1/2}} = g\frac{m}{A_o t} \quad (9)$$

The vapor deposition process was accomplished under the same experimental conditions for all compounds; the same equilibrium vapor pressure (≈ 0.3 Pa) and derived mass flow rate, as well as the deposition time (60 minutes), were applied. A

constant mass flow rate on the surface of the substrate (≈ 22 ng cm^{-2} s^{-1}) was regulated by the evaporation temperature of each compound. Regarding the morphological analysis (Fig. 10), the irregular topography of the quartz crystals is depicted by images (a)–(c). In all cases, the several cavities and the surface roughness of the quartz crystal have an important role for the nucleation and growth mechanisms as well as to the topography of thin films. There is perceptible differentiation in the topography of the three types of quartz crystals (Au, Ag, Al) used as the grain morphology of the coated metal is dissimilar. The structure and surface morphology of organic materials produced by vapor deposition methods, particularly the vacuum thermal evaporation, is highly dependent on the structural, thermal and morphological properties of the surface.[19,21,42,43,56,57,71–74] The morphology of vapor-deposited thin films of **mCP**, **CBP**, and **TCB** does not evidence a significant growth of crystal structures as the images suggest an amorphous appearance, with emphasis on **mCP**, accompanied by a high dependence with the substrate roughness. Looking at the SEM images, grains' shape and size are not recognized. SEM of an amorphous material doesn't release any features and no particles can be distinguished. These findings agree with a recent work regarding similar systems, upon which XRD was used to confirm the amorphous nature of thin films.[21] Strong binding of organic

thin films can be perceived and is a typical observation for as-deposited thin organic films growing by PVD methods.[21] Predictably, the large coverage and homogeneity of these organic materials indicate a layer-by-layer growth process.[75,76] One of the key properties for the amorphous nature of as-deposited films of phenylcarbazoles is the glass transition temperature (T_g). Literature reports indicate values of T_g of ≈ 330 K, ≈ 335 K, and ≈ 400 K for **mCP**,[77,78] **CBP**,[79,80] and **TCB**,[81,82] respectively. As the thin film deposition of this work were performed on surfaces kept at a constant temperature of 293 K, the amorphous nature of materials would be expected. The glassy state is usually observed for nonplanar molecules as the hard packing of molecules avoids the crystallization process. The ratio $T_g/T_m = 0.73$ ($\approx 3/4$) is observed for **mCP**, which would be expected due to the asymmetric nonplanar structure of this compound.[19] Lower values of T_g/T_m (0.61 for **CBP** and 0.67 for **TCB**) are typical for a more symmetric nonplanar structure, whose ratio of T_g/T_m is expected to be around 2/3.[19] The existence of a glassy state is also a consequence of the less flexibility of phenylcarbazole derivatives in comparison with some phenylamines. For instance, the higher flexibility of **TDAB** is related to the lower ability to form a glassy state. As discussed in previous reports, despite being nonplanar, due to the high flexibility (suitable ring rotation potential profile) this compound has a strong ability to crystallize (very lower liquid undercooling stability) which avoids the formation of the glassy state. Due to this fact, a vapor-deposited thin film of **TDAB** is always crystalline.[19,42,82]

Conclusions

The optical, morphological and thermodynamic behavior were explored for a series of carbazole derivatives (**mCP**, **CBP**, and **TCB**), organic semiconductors with wide use in molecular electronics and exciting liquid organic hydrogen carriers. The structural differentiation between phenylcarbazoles and phenylamine analogues was reflected in the physical chemistry behavior of each class of materials. Regarding the UV-vis characterization, phenylcarbazoles exhibit a blue shift compared to phenylamines, noticeably so as more moieties are present in the molecule, resulting in higher optical band gaps. From the thermodynamic study of phase transitions, it can be concluded that entropic factors are of greater importance for the higher melting points and low volatility exhibited by the solid phase of carbazole derivatives. Analysis of fusion and sublimation data suggests phenylcarbazoles retain higher levels of structuration when compared to their phenylamine counterparts. This trend also seems to persist after the melting point. The additional bond in phenylcarbazoles severely limits the freedom of movement of the end groups, resulting in less flexible structures that also remain partially interactive even after there is greater molecular mobility. From the morphological study of vapor-deposited phenylcarbazole thin films, it can be concluded that these compounds do not show significant crystal growth, as their smooth appearance strongly suggests it is largely amorphous. The experimental data reveals the role of the chemical bond between the phenyl groups in the carbazolyl unit for
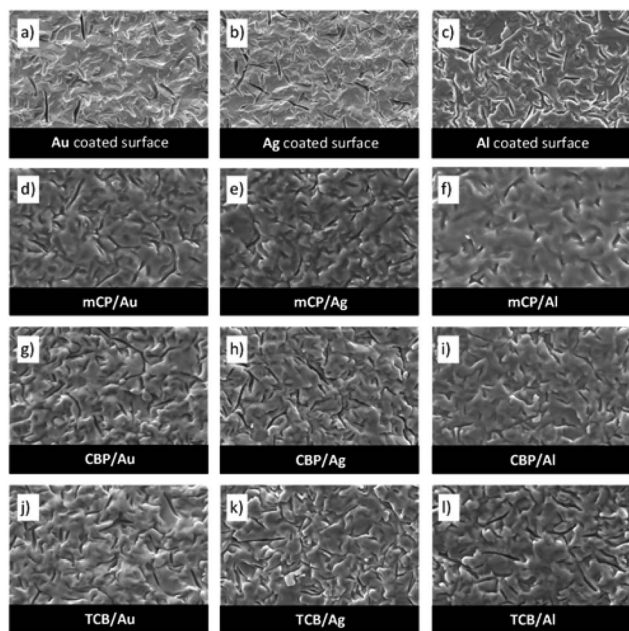

Fig. 10 Topographic images obtained by SEM of the vapor-deposited thin films produced in this work: gold (Au) coated quartz crystal surface (a); silver (Ag) coated quartz crystal surface (b); aluminium (Al) coated quartz crystal surface (c); thin film morphology of **mCP** deposited on Au (d), Ag (e), and Al (f); thin film morphology of **CBP** deposited on Au (g), Ag (h), and Al (i); thin film morphology of **TCB** deposited on Au (j), Ag (k), and Al (l). The thin films were deposited under the same experimental conditions: equilibrium vapor pressure of ≈ 0.3 Pa; mass flow rate at the substrate surface of ≈ 22 ng cm^{-2} s^{-1}; deposition time of 60 minutes; substrate temperature ≈ 293 K. For these experimental conditions, **mCP**, **CBP**, and **TCB** were evaporated at 472, 545, and 573 K, respectively.

a more rigid structure leading to the amorphous nature of thin films.

Conflicts of interest

There are no conflicts to declare.

Acknowledgements

References

1 V. Coropceanu, J. Cornil, D. A. da Silva Filho, Y. Olivier, R. Silbey and J.-L. Brédas, *Chem. Rev.*, 2007, **107**, 926–952.

2 N. T. Kalyani and S. J. Dhoble, *Renewable Sustainable Energy Rev.*, 2012, **16**, 2696–2723.

3 C. Wang, H. Dong, W. Hu, Y. Liu and D. Zhu, *Chem. Rev.*, 2012, **112**, 2208–2267.

4 J. C. S. Costa, R. J. S. Taveira, C. F. R. A. C. Lima, A. Mendes and L. M. N. B. F. Santos, *Opt. Mater.*, 2016, **58**, 51–60.

5 C. Wang, H. Dong, L. Jiang and W. Hu, *Chem. Soc. Rev.*, 2018, **47**, 422–500.

6 Y. Shirota, *J. Mater. Chem.*, 2000, **10**, 1–25.

7 Y. Shirota, K. Okumoto and H. Inada, *Synth. Met.*, 2000, **111**, 387–391.

8 Y. Tao, C. Yang and J. Qin, *Chem. Soc. Rev.*, 2011, **40**, 2943–2970.

9 J. Melas-Kyriazi, I.-K. Ding, A. Marchioro, A. Punzi, B. Hardin, G. F. Burkhard, N. Tétreault, M. Grätzel, J.-E. Moser and M. D. McGehee, *Adv. Energy Mater.*, 2011, **1**, 407–414.

10 L. Calió, S. Kazim, M. Grätzel and S. Ahmad, *Angew. Chem.*, 2016, **55**, 14522–14545.

11 Y. Shirota, *J. Mater. Chem.*, 2005, **15**, 75–93.

12 T. Leijtens, I.-K. Ding, T. Giovenzana, J. T. Bloking, M. D. McGehee and A. Sellinger, *ACS Nano*, 2012, **62**, 1455–1462.

13 M. Saliba, S. Orlandi, T. Matsui, S. Aghazada, M. Cavazzini, J.-P. Correa-Baena, P. Gao, R. Scopelliti, E. Mosconi, K.-H. Dahmen, F. De Angelis, A. Abate, A. Hagfeldt, G. Pozzi, M. Grätzel and M. K. Nazeeruddin, *Nat. Energy*, 2016, **1**, 15017.

14 Y. Kuwabara, H. Ogawa, H. Inada, N. Noma and Y. Shirota, *Adv. Mater.*, 1994, **6**, 677–679.

15 P. Agarwala and D. Kabra, *J. Mater. Chem. A*, 2017, **5**, 1348–1373.

16 R. Braveenth, H. Woo Bae, I. Jang Ko, W. Qiong, Q. P. B. Nguyen, P. G. S. Jayashantha, J. H. Kwon and K. Y. Chai, *Org. Electron.*, 2017, **51**, 463–470.

17 X. Liu, X. Shi, C. Liu, Y. Ren, Y. Wu, W. Yang, A. Alsaedi, T. Hayat, F. Kong, X. Liu, Y. Ding, J. Yao and S. Dai, *J. Phys. Chem. C*, 2018, **122**, 26337–26343.

18 G. Krucaite, D. Volyniuk, J. Simokaitiene, S. Grigalevicius, C.-H. Lin, C.-M. Shao and C.-H. Chang, *Dyes Pigm.*, 2019, **162**, 196–202.

19 J. C. S. Costa and L. M. N. B. F. Santos, *J. Phys. Chem. C*, 2013, **117**, 10919–10928.

20 K.-H. Lin, A. Prlj and C. Corminboeuf, *J. Mater. Chem. C*, 2018, **6**, 960–965.

21 J. C. S. Costa, A. Mendes and L. M. N. B. F. Santos, *J. Mater. Sci.*, 2018, **53**, 12974–12987.

22 R. F. Pineda, J. Troughton, M. Planells, I. S.-M. Santos, F. Muhith, G. S. Nichol, S. Haque, T. Watson and N. Robertson, *Phys. Chem. Chem. Phys.*, 2018, **20**, 1252–1260.

23 Y. Li, Y. Zhang, P. Heng, R. Shao, Y. Liu, W. Qiao, L. Wang and J. Zhang, *Org. Electron.*, 2018, **54**, 14–20.

24 S. Oner, M. Aydemir, F. Yesil, C. Sahin and C. Varlikli, *Dyes Pigm.*, 2018, **159**, 92–99.

25 C. Yin, J. Lu, Y. Xu, Y. Yun, K. Wang, J. Li, L. Jiang, J. Sun, A. D. Scully, F. Huang, J. Zhong, J. Wang, Y.-B. Cheng, T. Qin and W. Huang, *Adv. Energy Mater.*, 2018, **8**, 1800538.

26 A. Magomedov, S. Paek, P. Gratia, E. Kasparavicius, M. Daskeviciene, E. Kamarauskas, A. Gruodis, V. Jankauskas, K. Kantminiene, K. T. Cho, K. Rakstys, T. Malinauskas, V. Getautis and M. K. Nazeeruddin, *Adv. Funct. Mater.*, 2018, **28**, 1704351.

27 X. Liu, X. Ding, Y. Ren, Y. Yang, Y. Ding, X. Liu, A. Alsaedi, T. Hayat, J. Yao and S. Dai, *J. Mater. Chem. C*, 2018, **6**, 12912–12918.

28 X.-D. Zhu, X.-J. Ma, Y.-K. Wang, Y. Li, C.-H. Gao, Z.-K. Wang, Z.-Q. Jiang and L.-S. Liao, *Adv. Funct. Mater.*, 2019, **29**, 1807094.

29 S. H. Kim and J. Jang, *Appl. Phys. Lett.*, 2007, **90**, 223505.

30 M. Hu, Q. Xu, Y. Jiang, H. Mu, L. Gao, P. Hu, J. Huang and J. Su, *Dyes Pigm.*, 2018, **150**, 185–192.

31 S.-R. Park, S.-M. Kim, Y. Choi, J. Y. Lee, J.-H. Lee and M. C. Suh, *Dyes Pigm.*, 2019, **170**, 107621.

32 S. Gong, X. He, Y. Chen, Z. Jiang, C. Zhong, D. Ma, J. Qin and C. Yang, *J. Mater. Chem.*, 2012, **22**, 2894–2899.

33 M.-S. Gong, J.-R. Cha and C. W. Lee, *Org. Electron.*, 2017, **42**, 66–74.

34 C. Papp, P. Wasserscheid, J. Libuda and H.-P. Steinruck, *Chem. Rev.*, 2014, **14**, 879–896.

35 K. Stark, V. N. Emel'yanenko, A. A. Zhabina, M. A. Varfolomeev, S. P. Verevkin, K. Muller and W. Arlt, *Ind. Eng. Chem. Res.*, 2015, **54**, 7953–7966.

36 V. N. Emel'yanenko, M. A. Varfolomeev, S. P. Verevkin, K. Stark, K. Muller, M. Muller, A. Bosmann, P. Wasserscheid and W. Arlt, *J. Phys. Chem. C*, 2015, **119**, 26381–26389.

37 K. Stark, P. Keil, S. Schug, K. Muller, P. Wasserscheid and W. Arlt, *J. Chem. Eng. Data*, 2016, **61**, 1441–1448.

38 I. Y. Choi, B. S. Shin, S. K. Kwak, K. S. Kang, C. W. Yoon and J. W. Kang, *Int. J. Hydrogen Energy*, 2016, **41**, 9367–9373.

39 V. N. Emel'yanenko, D. H. Zaitsau, A. A. Pimerzin and S. P. Verevkin, *J. Chem. Thermodyn.*, 2019, **132**, 122–128.

40 K. R. Jiang, *Thin Solid Films*, 1990, **191**, 91–126.

41 S. M. Rossnagel, *J. Vac. Sci. Technol., A*, 2003, **21**, S74.

42 J. C. S. Costa, R. M. Rocha, I. C. M. Vaz, M. C. Torres, A. Mendes and L. M. N. B. F. Santos, *J. Chem. Eng. Data*, 2015, **60**, 3776–3791.

43 J. C. S. Costa, J. Azevedo, L. M. N. B. F. Santos and A. Mendes, *J. Phys. Chem. C*, 2017, **121**, 2080–2087.

44 J. Oh, R. Zhang, P. P. Shetty, J. A. Krogstad, P. V. Braun and N. Miljkovic, *Adv. Funct. Mater.*, 2018, **28**, 1707000.

45 M. Kurahashi, M. Fukuyo and A. Shimada, *Bull. Chem. Soc. Jpn.*, 1969, **42**, 2174–2179.

46 A. N. Sobolev, V. K. Belsky, I. P. Romm, N. Y. Chernikova and E. N. Guryanova, *Acta Crystallogr.*, 1985, **C41**, 967–971.

47 M. E. Wieser, N. Holden, T. B. Coplen, J. K. Bohlke, M. Berglund, W. A. Brand, P. De Bièvre, M. Groning, R. D. Loss, J. Meija, T. Hirata, T. Prohaska, R. Schoenberg, G. O'Connor, T. Walczyk, S. Yoneda and X. K. Zhu, *Pure Appl. Chem.*, 2013, **85**, 1047–1078.

48 R. Sabbah, A. Xu-wu, J. S. Chickos, M. L. Planas Leitão, M. V. Roux and L. A. Torres, Reference Materials for Calorimetry and Differential Thermal Analysis, *Thermochim. Acta*, 1999, **331**, 93–204.

49 M. V. Roux, M. Temprado, J. S. Chickos and Y. Nagano, *J. Phys. Chem. Ref. Data*, 2008, **37**, 1855–1996.

50 L. M. N. B. F. Santos, L. M. S. S. Lima, C. F. R. A. C. Lima, F. D. Magalhães, M. C. Torres, B. Schröder and M. A. V. Ribeiro da Silva, *J. Chem. Thermodyn.*, 2011, **43**, 834–843.

51 L. M. N. B. F. Santos, A. I. M. C. Lobo Ferreira, V. Stejfa, A. S. M. C. Rodrigues, M. A. A. Rocha, M. C. Torres, F. M. S. Tavares and F. S. Carpinteiro, *J. Chem. Thermodyn.*, 2018, **126**, 171–186.

52 M. A. V. Ribeiro da Silva, M. J. S. Monte and L. M. N. B. F. Santos, *J. Chem. Thermodyn.*, 2006, **38**, 778–787.

53 S. P. Verevkin, *J. Chem. Thermodyn.*, 1997, **29**, 1495–1501.

54 L. Malaspina, G. Bardi and R. Gigli, *J. Chem. Thermodyn.*, 1974, **6**, 1053–1064.

55 N. Wakayama and H. Inokuchi, *Bull. Chem. Soc. Jpn.*, 1967, **40**, 2267–2271.

56 J. C. S. Costa, A. F. S. M. G. Coelho, A. Mendes and L. M. N. B. F. Santos, *Appl. Surf. Sci.*, 2018, **428**, 242–249.

57 J. C. S. Costa, J. Azevedo, J. P. Araújo, L. M. N. B. F. Santos and A. Mendes, *Thin Solid Films*, 2018, **664**, 12–18.

58 J. Sworakowski, *Synth. Met.*, 2018, **235**, 125–130.

59 S. B. Suryawanshi, P. G. Mahajan, A. J. Bodake, G. B. Kolekar and S. R. Patil, *Spectrochim. Acta, Part A*, 2017, **183**, 232–238.

60 L.-S. Cui, S.-C. Dong, Y. Liu, Q. Li, Z.-Q. Jiang and L.-S. Liao, *J. Mater. Chem. C*, 2013, **1**, 3967–3975.

61 K. L. Woon, A. Ariffin, K. W. Ho and S.-A. Chen, *RSC Adv.*, 2018, **8**, 9850–9857.

62 I. A. Wright, H. A. Al-Attar, A. S. Batsanov, A. P. Monkman and M. R. Bryce, *Phys. Chem. Chem. Phys.*, 2018, **20**, 11867–11875.

63 R. K. Konidena, K. H. Lee and J. Y. Lee, *Chem. Commun.*, 2019, **55**, 8178–8181.

64 J. C. S. Costa and L. M. N. B. F. Santos, *J. Chem. Eng. Data*, 2019, **64**, 2229–2246.

65 J. Chickos and D. Lipkind, *J. Chem. Eng. Data*, 2008, **53**, 2432–2440.

66 J. S. Chickos, *Thermochim. Acta*, 1998, **313**, 19–26.

67 W. E. Acree, *Thermochim. Acta*, 1993, **219**, 97–104.

68 W. V. Steele, *J. Chem. Thermodyn.*, 1978, **10**, 441–444.

69 C. F. R. A. C. Lima, M. A. A. Rocha, A. Melo, L. R. Gomes, J. N. Low and L. M. N. B. F. Santos, *J. Phys. Chem. A*, 2011, **115**, 11876–11888.

70 J. C. S. Costa, A. Mendes and L. M. N. B. F. Santos, *J. Chem. Eng. Data*, 2018, **63**, 1–20.

71 Z. Luo, Y. Lu, D. W. Singer, M. E. Berck, L. A. Somers, B. R. Goldsmith and A. T. C. Johnson, *Chem. Mater.*, 2011, **23**, 1441–1447.

72 J. Munemasa and T. Kumakiri, *Surf. Coat. Technol.*, 1991, **49**, 496–499.

73 M. Nisha, S. Anusha, A. Antony, R. Manoj and M. K. Jayaraj, *Appl. Surf. Sci.*, 2005, **252**, 1430–1435.

74 A. A. Virkar, S. Mannsfeld, Z. Bao and N. Stingelin, *Adv. Mater.*, 2010, **22**, 3857–3875.

75 J. A. Venables, G. D. T. Spiller and M. Hanbucken, *Rep. Prog. Phys.*, 1984, **47**, 399–459.

76 Z. Zhang and M. G. Lagally, *Science*, 1997, **276**, 377–383.

77 M.-S. Gong, J.-R. Cha and C. W. Lee, *Org. Electron.*, 2017, **42**, 66–74.

78 D. Sun, Z. Yang, Z. Ren, H. Li, M. R. Bryce, D. Ma and S. Yan, *Chem.–Eur. J.*, 2014, **20**, 16233–16241.

79 D. Hu, P. Lu, C. Wang, H. Liu, H. Wang, Z. Wang, T. Fei, X. Gu and Y. Ma, *J. Mater. Chem.*, 2009, **19**, 6143–6148.

80 T. Zhang, Y. Liang, J. Cheng and J. Li, *J. Mater. Chem. C*, 2013, **1**, 757–764.

81 W. Jiang, Z. Ge, P. Cai, B. Huang, Y. Dai, Y. Sun, J. Qiao, L. Wang, L. Duan and Y. Qiu, *J. Mater. Chem.*, 2012, **22**, 12016–12022.

82 Y. Shirota, *J. Mater. Chem.*, 2000, **10**, 1–25.